Scientific Research Publishing

Advances in Aerospace Science and Technology, 2020, 5, 85-99
https://www.scirp.org/journal/aast
ISSN Online: 2473-6724
ISSN Print: 2473-6708

Numerical Analysis and Modelling of a 100 N Hypergolic Liquid Bipropellant Thruster

Grace Olileanya Ngwu[1], Benjamin Iyenagbe Ugheoke[1], Olatunbosun Tarfa Yusuf[2], Mopa Ashem Nyabam[2], Spencer Ojogba Onuh[3*]

[1]Department of Mechanical Engineering, University of Abuja, Abuja, Nigeria
[2]National Space Research and Development Agency, Abuja, Nigeria
[3]Department of Mechanical Engineering, University of Maiduguri, Maiduguri, Borno State, Nigeria
Email: *onuh.spencer@cstd.nasrda.gov.ng

How to cite this paper: Ngwu, G.O., Ugheoke, B.I., Yusuf, O.T., Nyabam, M.A. and Onuh, S.O. (2020) Numerical Analysis and Modelling of a 100 N Hypergolic Liquid Bipropellant Thruster. *Advances in Aerospace Science and Technology*, **5**, 85-99.
https://doi.org/10.4236/aast.2020.54006

Received: October 28, 2020
Accepted: November 27, 2020
Published: November 30, 2020

Abstract

This study focuses on the stepwise procedure involved in the development of a numerical model of a bi-propellant hypergolic chemical propulsion system using key features and performance characteristics of existing and planned (near future) propulsion systems. The study targets specific impulse of 100 N delivery performance of thrust chambers which is suitable for primary propulsion and attitude control for spacecraft. Results from numerical models are reported and validated with the Rocket Propulsion Analysis (RPA) computation concept. In the modelling process, there was proper consideration for the essential parts of the thruster engine such as the nozzle, combustion chamber, catalyst bed, injector, and cooling jacket. This propulsion system is designed to be fabricated in our next step in advancing this idea, using a combination of additive manufacturing technology and commercial off the shelf (COTS) parts along with non-toxic propellants. The two non-toxic propellants being considered are Hydrogen Peroxide as the oxidiser and Kerosene as the fuel, thus making it a low-cost, readily available and environmentally-friendly option for future microsatellite missions.

Keywords

Bi-Propellant, Hypergolic Chemical, Thrust Chambers, Hydrogen Peroxide, Additive Manufacturing, Rocket Propulsion Analysis

1. Introduction

In the fields of engineering and technology, recent advances have been made, such as additive manufacturing, micro fluidics, Micro Electro Mechanical Systems (MEMS), low power microelectronics, high efficiency solar cells, and ad-

vanced materials [1], and have led to an increased interest by aerospace industries across the World in developing its near future generation spacecraft. These aerospace industries have incorporated these advances to achieve more complex missions and high performances at a low cost that would be practically impossible or financially prohibitive using traditional spacecraft. These spacecrafts such as satellites, rocketry, space probes, are being developed for numerous applications related to research and development, defence and industry. Satellite subsystems consist of Payloads, Telemetry, Tracking & Control (TT & C), Thermal control, Attitude and Orbit Control Subsystem (AOCS), On-Board Data Handling (OBDH), Structure, Power subsystem and Propulsion system [2].

Spacecraft propulsion is characterised in general by its complete integration within the spacecraft as an integral part of attitude manoeuvre and stabilisation of satellite. It functions to provide forces and torques to place satellites into orbit when used in launch vehicles as primary propulsion systems, send satellites to the moon or the planets in interplanetary mission, position, adjust and maintain orbits of spacecraft by orbit control and orient spacecraft by attitude control when used as secondary propulsion systems [3]. The achievement of the attitude and orbit operational requirements of spacecraft (e.g. satellites, spacecraft propulsion systems) is characterised in particular by the following [4]:

- Low thrust levels (1 mN to 500 N) with low acceleration levels
- Continuous operation mode for orbit control
- Pulsed operation mode for attitude control
- Predictable, accurate and repeatable performance (impulse bits)
- Reliable, leak-free long-time operation (storable propellants)
- Minimum and predictable plume impingement effects

Among the classification of spacecraft propulsion systems that most commonly used are chemical propulsion systems, owing to their simplicity, reliability, and low power requirements [5]. It is based on the principle of converting chemical energy to kinetic energy of the exhaust gases in a nozzle [6]. Liquid propulsion systems are suitable as primary propulsion and attitude control thrusters, as this paper demonstrates our recent efforts to design and build a low thrust level of 100 N using hypergolic bi-propellant liquid for attitude control. **Figure 1** shows a typical bipropellant system applied as rocket engine; it consists of a combination of fuel (Kerosene) and oxidisers (Hydrogen Peroxide) which are pressure-fed into a combustion chamber through a valve that mixes the fluids and initiate combustion (self-ignites at room temperature), with the products ejected through a converging-diverging nozzle to give the target thrust. Hydrogen Peroxide and Kerosene were selected as the propellants in this text, after careful consideration of the Elements of Rocket Propulsion, chemical properties and its eco-friendliness. The oxidiser, hydrogen peroxide is cheap and easy to find; this is due to the hypergolic nature of the propellants.

The critical physical features and flow scheme of basic spacecraft bipropellant propulsion system consists of: 1) fuel and oxidiser tanks, 2) injector, 3) pressure regulator, 4) ignition system, 5) pipes of varying dimensions, 6) pressure

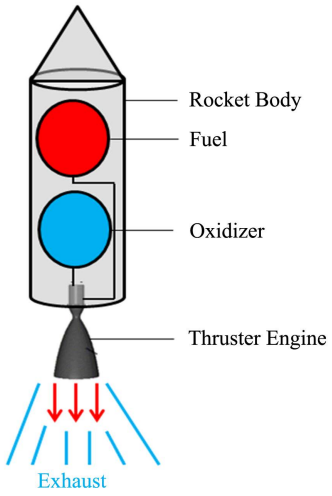

Figure 1. Basic bipropellant propulsion system.

regulator and valves, 7) fill and drain valves, 8) thruster engine (combustion chamber and nozzle section), coolant and coolant jacket. **Figure 2** shows a flow scheme of the bipropellant system.

In this work, the numerical analysis and modelling overview of a 100 N thrust propulsion system are presented along with supporting results from preliminary Rocket Propulsion Analysis (RPA) simulation to demonstrate and verify the concept. This paper presents the primary propulsion mathematical equations used to arrive at our design/operating/performance parameters and describes the selection of the fuel/oxidiser combination in bipropellant operation for application in satellites attitude control.

2. Materials and Methods

2.1. Propellant Mechanism Overview

The propellants of choice are Kerosene as fuel and hydrogen peroxide as the oxidiser, these were considered owing to their significant cost saving, readily available (easy to find), clean and safe (non-toxic) and non-cryogenic to avoid complexity in our engine design [7] [8]. For propulsion system based on kerosene ($C_{12}H_{26}$) and hydrogen peroxide (H_2O_2) bipropellant, the equation for the reaction is as shown in Equation (1):

$$H_2O_{2_{(l)}} + \text{Kerosene}_{(l)} \rightarrow 12O_{2_{(g)}} + (n+1)H_2O_{(g)} + \text{heat}_{(l)} \quad (1)$$

Here, n represents a mole fraction of water present in the hydrogen peroxide fuel; typically, the hydrogen peroxide concentrations range 85% - 90% by mass. In this propulsion design, the chemical decomposition of the hydrogen peroxide is achieved using a homogeneous catalysis approach wherein the catalyst reacts with the hydrogen peroxide in the liquid phase [9]. The resulting exothermic reaction produces high-temperature gaseous products that are subsequently passed through a converging-diverging supersonic nozzle to produce the desired thrust. The equation for this reaction is given in Equation (2):

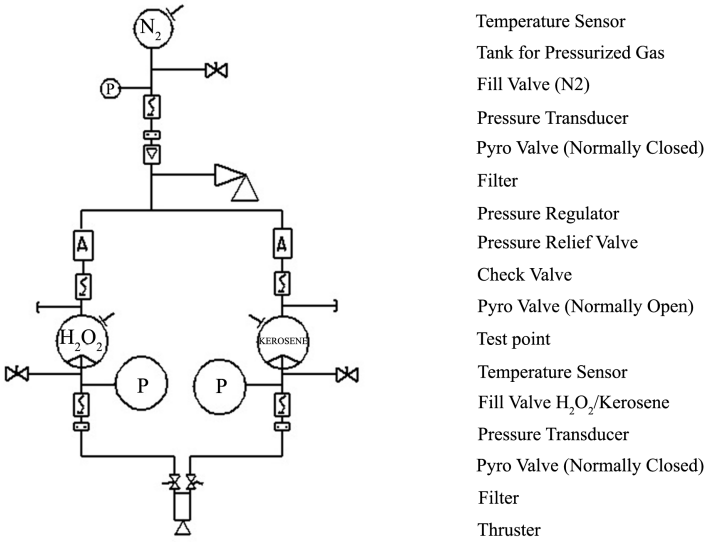

Figure 2. Flow scheme of bipropellant systems.

$$H_2O_{2_{(l)}} \xrightarrow{\text{catalyst}} 2H_2O_{(l)} + O_{2_{(g)}} + \text{Heat} \quad (2)$$

A high-level representation of this process is shown schematically in **Figure 3**.

From the storage vessels, high test hydrogen peroxide and Kerosene are fed into the mixing chamber, in which a chemical reaction that produces gaseous products, takes place. The generated gaseous products are then expelled through a converging-diverging nozzle.

The storage, mixing and reaction, and expulsion are the three main stages of this propulsion concept. First, in the storage stage, the kerosene and hydrogen peroxide are both stored separately in chemically compatible vessels to be pressurised by nitrogen gas, as shown in **Figure 3**. In this system, the storage vessels are pressurized by the slowly controlled nitrogen gas; this increases pressure in the storage vessels of hydrogen peroxide and Kerosene. The hydrogen peroxide passes through a catalyst (manganese oxide, metallic silver, rhodium, palladium, platinum or gold) for self-decomposition and to enhance the performance of the thruster [10]. For this study, the catalyst chosen is manganese oxide (MnO_2) as a result of its availability and lower cost as compared to the others. Here, the catalyst solution mixes with the hydrogen peroxide resulting in a fast decomposition reaction. This reaction produces steam, oxygen, and heat. The catalyst solvent is vapourised through the heat released by the decomposition reaction. The generated high temperature created by the decomposition reaction results in secondary combustion process as the catalyst solvent vapours react with oxygen. Consequently, there is a release of additional thermal energy into the flow, thereby increasing the I_{sp} of the propulsion system, which is a significant aspect of this design.

The second stage (mixing and reaction), happens when kerosene and hydrogen peroxide (having undergone self-decomposition) is allowed to flow into the mixing and reaction chamber of the thruster [11] [12].

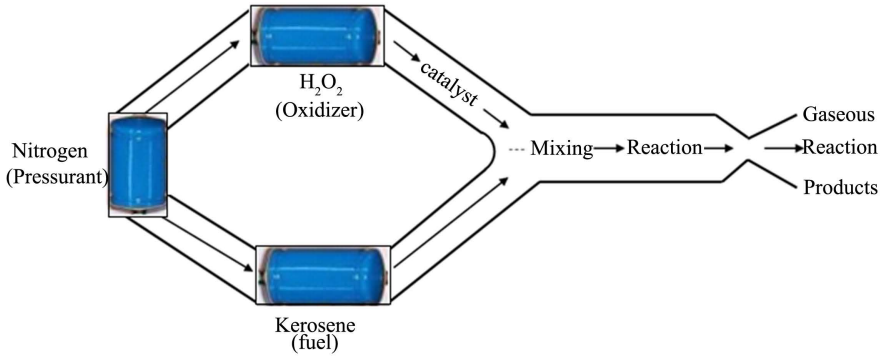

Figure 3. Representation of propellant mechanism.

Following the occurrence of the reactions in the second stage, the third stage of the propulsion system, which is the expulsion stage, becomes activated at the converging-diverging nozzle. The decrease in the mass density of the gaseous reaction products compared to the liquid density results in a significant increase in the pressure inside the chamber for the mixing and reaction. This pressure pushes the generated products through the converging-diverging nozzle to achieve supersonic conditions and thereby generating the thrust. The total mass flow rate of propellants that will give rise to the expected thrust is given by Equation (3) [13] [14].

$$E_{mfr} = \frac{\text{Thrust}}{I_{sp}} \tag{3}$$

where E_{mfr} is the total mass flow rate, I_{sp} is the specific impulse.

Based on that total, we will determine which part of the propellant mass is fuel and which part is the oxidiser. Given the oxidiser/fuel ratio of 7.35, the mass flow ratios can be determined using Equations (4) and (5):

$$M_f = \frac{E_{mfr}}{R+1} \tag{4}$$

$$M_o = \frac{E_{mfr}R}{R+1} \tag{5}$$

where M_f and M_o are the mass flow rates of the fuel and the oxidiser respectfully, R is the mixture ratio.

As the thruster generates heat, the combustion chamber and the nozzle will require cooling. The majority of the heat transfer from the combustion chamber wall is by convection compared to radiation and conduction (which are small). The design is such that the cooling jacket is roundabout the thruster with water serving as a coolant. The water is at a steady flow with a flow rate high enough to prevent boiling in the cooling jacket. The cooling jacket will consist of inner and outer walls. The space between the walls will serve as a passage for the coolant (water) to flow. The summarized theoretical basic operating parameters of the engine are in **Table 1** (The theoretical basic operating parameters of the thrust engine), from which we can determine the materials to use and physical dimensions of the thrust chamber and nozzle.

Table 1. The theoretical basic operating parameters of the thrust engine [4].

Propellants Combination Oxidiser/Fuel	Combustion Pressure (MPa)	Mixture Ratio (R)	Flame Temperature (K)	I_{sp} (S)	Thrust (N)	Total Mass Flow (Oxidizer + Fuel) (g/s)
H_2O_2/Kerosene	1.277	7.35	266.7	273	100	37.3516

2.2. System Design Overview

With the vital propulsion system operating parameters identified, we determine chamber dimensions, nozzle outlet diameter, expansion ratios, throat diameter, by first determining some gas values [15]. The idea is to transform a high pressure, high temperature, low-velocity gas, like the combustion products, into a low pressure, relatively low temperature, and high-speed gas. First, we determine the temperature of the gas in the nozzle throat (T_{throat}) using Equation (6), as the gas temperature at the nozzle throat must be less than in the combustion chamber due to loss of some thermal energy during the attainment of the local speed of sound (Mach number of 1) by the gas at the throat.

$$T_{\text{throat}} = T_{\text{chamber}}\left[\frac{1}{1+\frac{\gamma-1}{2}}\right] \tag{6}$$

where T_{throat} is the temperature at the throat, T_{chamber} is the temperature of the chamber, and γ is the specific heat ratio.

The ratio of the specific heat for the gas is represented by Gamma (γ); it relates to the heat capacity at a given volume for a gas [16]. For the products of kerosine and hydrogen peroxide combustion, Gamma equals 266.7.

Now, the gas pressure at the nozzle throat can be determined. The pressure at the nozzle throat must be less than in the combustion chamber due to attainment of the local speed of sound (Mach number of 1) by the gas at the throat, as shown in Equation (7):

$$P_{\text{throat}} = P_{\text{chamber}}\left[1+\frac{\gamma-1}{2}\right]^{\frac{-\gamma}{\gamma-1}} \tag{7}$$

where P_{throat} is the pressure at the throat and P_{chamber} is the pressure at the chamber.

Equation (8) was used to obtain the engine throat diameter, after determining the gas parameters such as temperature and pressure at the throat.

$$A_{\text{throat}} = \frac{E_{mfr}}{P_{\text{throat}}\sqrt{\left(\frac{R}{M}\right)T_{\text{throat}}/\gamma G_c}} \tag{8}$$

where A_{throat} is the area of the throat, R is the universal gas constant, M is the molecular weight of the exhaust gasses, and G_c is the universal gravitation constant.

Given this area, the diameter is determined using Equation (9), by the simple geometry of circles:

$$D_{\text{throat}} = \sqrt{4A_{\text{throat}}/\pi} \tag{9}$$

where D_{throat} is the diameter of the throat.

The Mach number speed of the exhaust gasses is obtained to determine exhaust area (A_{exhaust}) that will yield exhaust pressure equal to the local atmospheric pressure for that Mach number (M_e).

$$M_e^2 = \frac{2}{\gamma - 1}\left[\left(\frac{P_{\text{chamber}}}{P_{\text{atm}}}\right)^{\frac{\gamma-1}{\gamma}} - 1\right] \tag{10}$$

where P_{atm} is atmospheric pressure.

The area of the exhaust is given by Equation (11):

$$A_{\text{exhaust}} = \frac{A_{\text{throat}}}{M_e}\left[\frac{1 + \frac{\gamma-1}{2}M_{\text{exhaust}}^2}{\frac{\gamma+1}{2}}\right]^{\frac{\gamma+1}{2(\gamma-1)}} \tag{11}$$

In calculating the nozzle inlet diameter, the reality is that the nozzle inlet and chamber outlet dimensions are the same. With this, the volume of the chamber (V_{chamber}) is given by Equation (12):

$$V_{\text{chamber}} = L^* * A_{\text{throat}} \tag{12}$$

where L^* is a characteristic length specific to the type of propellant used. In this case the characteristic length, L^* = 1.778 m.

From which the chamber length (L_{chamber}) is derived from Equation (13):

$$L_{\text{chamber}} = \frac{V_{\text{chamber}}}{1.1 * A_{\text{chamber}}} \tag{13}$$

The length of the nozzle (L_{nozzle}) can be calculated using the given formula in Equation (14):

$$L_{\text{nozzle}} = \frac{D_{\text{exhaust}} - D_{\text{throat}}}{2 * \tan\theta} \tag{14}$$

where D_{exhaust} is the exhaust diameter, D_{throat} is the throat diameter, and θ is the nozzle half-angle in radians.

The gas (combustion products) pressure and physical dimensions of the thruster engine are summarised in **Table 2** (The theoretical basic design parameters of the engine). **Figure 4** shows the schematic design of the 100 N thruster while **Figure 5** shows the 3D solid model of the thruster engine for further experimental usage.

To keep the temperatures of the thruster engine within reasonable value to avoid debilitating the metals wall of the combustion chamber to the point at which they cannot resist the chamber pressure anymore, we devised a means using active cooling to keep the temperatures within a reasonable limit. The cooling was achieved using a cooling fluid (water) circulated inside a cooling jacket against the engine walls to get heat out of the engine as shown in **Figure 6**.

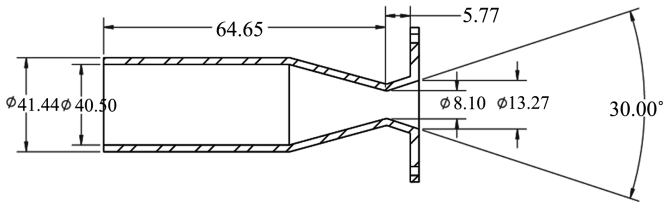

Figure 4. Schematic of the 100 N thruster. Dimensions are in mm.

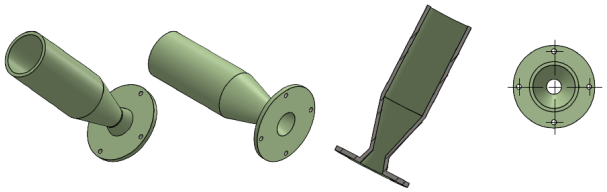

Figure 5. Solid model of the thruster engine.

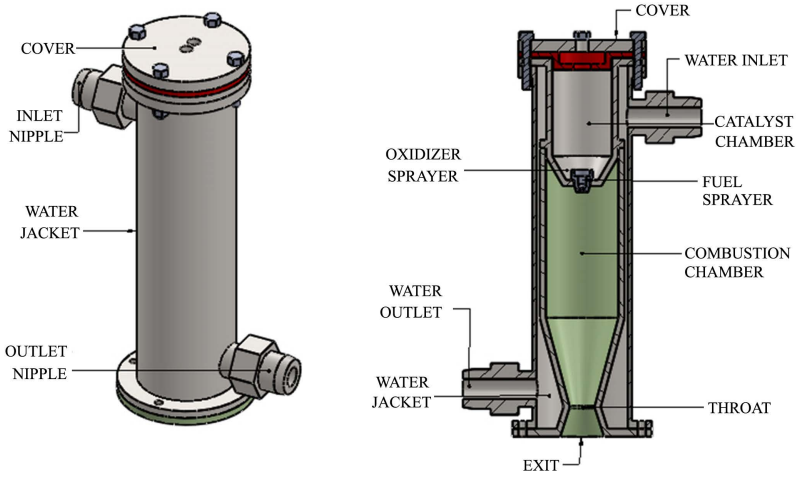

Figure 6. Solid model of the thruster engine with watercoolant jacket.

Table 2. The theoretical basic design parameters of the engine.

Parameter	Value
Gamma (γ)	1.1823
Throat Gas Pressure (MPa)	0.7249
Throat Area (mm^2)	51.5270
Throat Diameter (mm)	8.0998
Exhaust gas velocity (Mach)	2.29024
Nozzle exit area (mm^2)	138.1979
Nozzle exit diameter (mm)	13.2650
Length of Nozzle (mm)	9.6384
Chamber Volume (mm^3)	91,615.006
Chamber Diameter (mm)	40.499
Chamber Area (mm^2)	1288.3528
Chamber Length (including Convergent Segment) (mm)	64.6456
Chamber Wall thickness (mm)	0.4688
Nozzle Half-Angle (˚C)	15˚

3. Results and Discussion

3.1. Performance Characterisation Using Rocket Propulsion Analysis

Rocket Propulsion Analysis (RPA) is a multi-platform analysis tool intended for use in conceptual and preliminary design phases of rocket engines. It describes the numerical models and computation techniques of the design, to estimate the expected performance of thrust chambers. All the operation parameters obtained from our analytical calculations based on the expected thrust are subjected to Rocket Propulsion Analysis (RPA) to validate the performance of the thrust engine. The results obtained are subsequently discussed.

3.2. Thrust and Mass Flow Rates

The simulated results showed that with a 85% concentration of hydrogen peroxide, a chamber thrust of 97.62 N was obtained with a specific impulse of 230.85 s and a total mass flow rate of 43.12 g/s. Figure 7 shows simulated chamber geometry with the conical nozzle. Table 3 shows simulated results using RPA.

From Figure 7, the geometry of the thrust chamber with the conical nozzle using RPA are: D_c = 40.50 mm, b = 30.00 deg, R_2 = 57.43 mm, R_1 = 6.07 mm, L^* = 1128.40 mm, L_c = 65.00 mm, L_{cyl} = 19.92 mm, D_t = 8.10 mm, R_n = 1.55 mm, T_e = 15.00 deg, L_e = 9.84 mm and D_e = 13.26 mm.

An increase in the diameter of the nozzle (exhaust) led to a significant improvement of the thrust. There is a need for the rise in the nozzle diameter (Dexhaust) to achieve the desired thrust with an exit pressure matching the

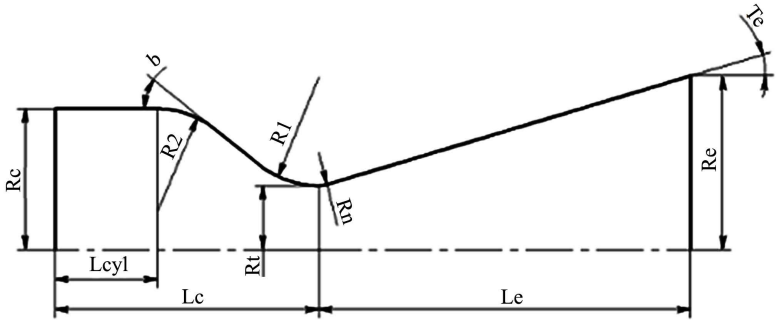

Figure 7. Geometry of thrust chamber with conical nozzle from RPA.

Table 3. Calculated result simulated using RPA.

Propellants Combination Oxidiser/Fuel	Parameter	Value
H_2O_2/Kerosene	Chamber thrust (vac)	97.97 N
	Specific impulse (vac)	235.91868 s
	Total mass flow rate	42.34 g/s
	Oxidizer mass flow rate	37.27 g/s
	Fuel mass flow rate	5.07 g/s

ambient pressure ($P_{exit} = P_{atm}$). Furthermore, this will mean an increased expansion ratio.

From simulated results (RPA), an expansion ratio of 3.232 and a nozzle diameter of 14.56 mm produced the desired thrust of 100 N, with a specific impulse of 236.49 s. Figure 8 (simulated using RPA) shows the geometry of the thrust chamber and the conical nozzle. Table 4 shows the results obtained from an increased expansion ratio, ε using RPA. A comparative summary between the calculated results and those obtained from an increased expansion ratio is shown in Table 5 (Comparative summary between calculated results and simulated results from increased expansion ratio, ε).

From Figure 8, the geometry of the thrust chamber with the conical nozzle using RPA are: $D_c = 40.50$ mm, $b = 30.00$ deg, $R_2 = 57.43$ mm, $R_1 = 6.07$ mm, $L^* = 1128.40$ mm, $L_c = 65.00$ mm, $L_{cyl} = 19.92$ mm, $D_t = 8.10$ mm, $R_n = 1.55$ mm, $T_e = 15.00$ deg, $L_e = 12.26$ mm and $D_e = 14.56$ mm.

It is worthy of note that a rise in the concentration of the hydrogen peroxide gave a slight increase in the specific impulse with the range of 0.48% - 1.3%.

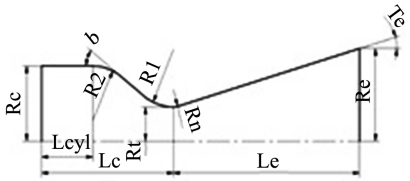

Thrust and mass flow rates

Chamber Thrust (vac)	0.10000	KN
Specific impulse (vac):	236.48804	s
Chamber Thrust (opt):	0.08674	KN
Specific Impulse (opt):	205.11296	s
Total mass flow rate:	0.04312	Kg/s
Oxidzer mass flow rate:	0.03796	Kg/s
Fuel Mass flow rate:	0.00516	Kg/s

Geometry of thrust Chamber with conical nozzle

D_C =	40.50	mm	L_e = 12.26	mm
R_2 =	57.43	mm	D_e = 14.56	mm
L^* =	1128.40	mm	b = 30.00	deg
L_C =	65.00	mm	R_1 = 6.07	mm
D_1 =	8.10	mm	L_{cyl} = 19.92	mm
R_n =	1.55	mm	T_e = 15.00	deg

Figure 8. Geometry of thrust chamber with conical nozzle with expansion ratio, ε.

Table 4. Simulated results from increased expansion ratio, ε.

Propellants Combination Oxidiser/Fuel	Parameter	Value
H_2O_2/ Kerosene	Chamber thrust (vac)	100 N
	Specific impulse (vac)	236.48804 s
	Total mass flow rate	43.12 g/s
	Oxidizer mass flow rate	37.96 g/s
	Fuel mass flow rate	5.156 g/s

Table 5. Comparative summary between calculated results and simulated results from increased expansion ratio, ε.

Propellants Combination Oxidiser/Fuel	Parameter (s)	Calculated Results	Simulated Results (RPA)
H_2O_2/Kerosene	Thrust (N)	100 (Expected)	97.62
	Specific Impulse (S)	273 (Assumed)	230
	Total Mass Flow Rate (g/s)	37. 35	43.12

3.3. Specific Impulse and Component Ratio

The component ratio is the ratio of oxidiser to fuel. As hypergolic fuels undergo spontaneous reactions, it thereby generates tremendous expansion resulting in high thrust. The mixture ratio of the oxidiser and the fuel is essential in determining the thrust. **Figure 9** shows that for component ratios of up to 5.5 as compare to 7.35 gotten from calculations. A similar outcome from simulated and calculated results was observed with a marginal increase between 5.5 and 7.35. Beyond a component ratio of 5.5, there is a steady fall in the specific impulse. Hence, for future works, a component ratio of 5.5 can be considered.

3.4. Heat Flux of the Thruster

Liquid thrusters are broadly used in space applications particularly for orbital maneuvers and launch vehicles. Optimization of complicated engineering systems has perpetually been a primary part of the design and to develop an ideal solution using modern designing methods through multidisciplinary design optimization (MDO); however, thermal-control and cooling are among the vital disciplines of the bi-propellant propulsion in multidisciplinary design optimization. The function of a thermal-control is to sustain all thrusters' components within the permissible temperature. It is only obtained by the control of heat fluxes from a combustion chamber. Due to high combustion temperatures and high heat flux rates from the hot gases to the chamber wall, thruster cooling is a significant design consideration.

For efficiency reasons, higher temperatures are desirable for optimal thruster performance, but materials lose their strength if the temperature becomes too high. Because of the large thermal capacity and the thermal inertia of the combustion chamber wall, its temperature will vary. The interaction of the boundary layer with the wall causes heat flux to the wall and change in parameters of the boundary layer.

In thrusters, the heat fluxes that can pass through the walls are quite high. Heat fluxes are generally in the range of 1 - 200 MW/m^2. The highest heat fluxes are found at the throat (Region B in **Figure 10**), which often sees twice the value of which is found in the associated chamber (Region A in **Figure 10**) and nozzle (Region C in **Figure 10**). The high temperature can be attributed to a thin boundary layer as a result of high speed, as seen in **Figure 10**. For a more significant part of the combustion chamber (Region A), both the convective and

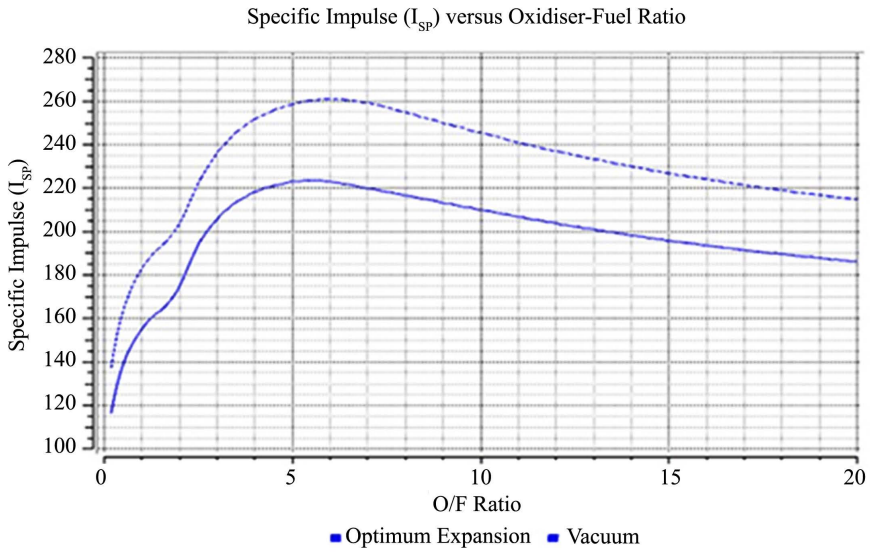

Figure 9. Specific impulse and component ratio.

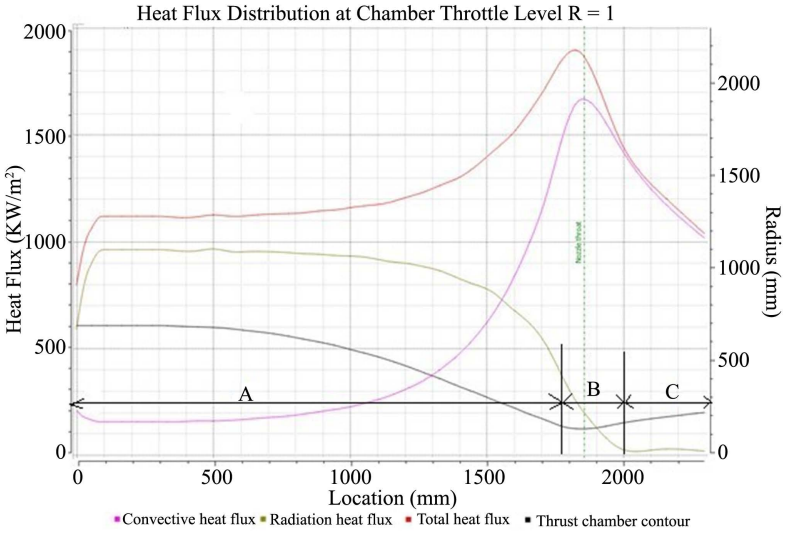

Figure 10. Heat distribution of the thruster.

radiative heat fluxes remain at around 200 and 950 KW/m^2 respectively. However, at the throat (Region B), the heat convective flux increases rapidly to 1.750 MW/m^2 while the Radiation heat flux is expected to drop to within the range of 100 - 400 KW/m^2. The convective heat flux is expected to drop as the hot gasses move through the nozzle to the exit; the radiative heat flux will be about 100 KW/m^2.

3.5. Temperature Distribution of the Thruster

The simulation results, as shown in **Figure 11**, indicate that the two measured temperature parameters show a similar profile. The results further show that both temperature profiles initialized at around 2000 - 2200 K. This initialization continued halfway into the chamber and then increased at the throat, attaining a

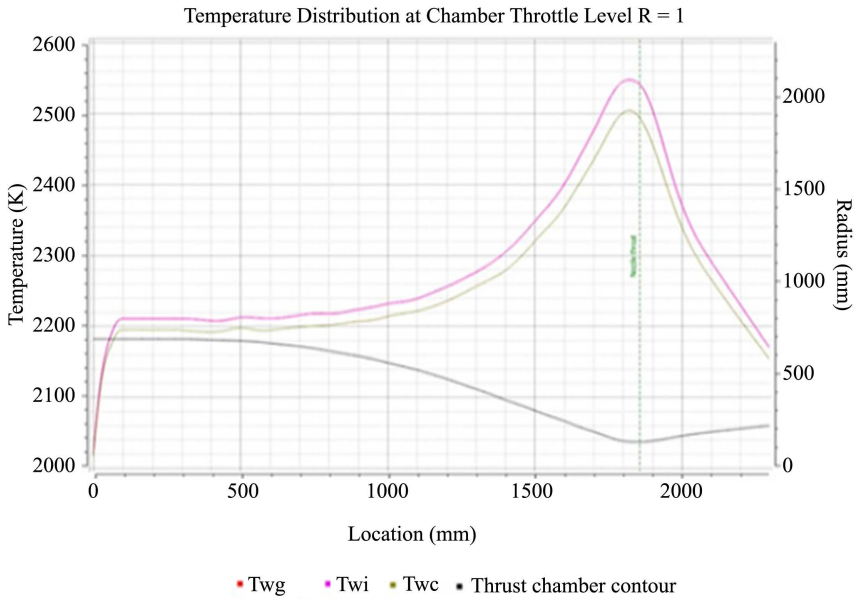

Figure 11. Temperature distribution at the chamber. Note: "T_{wg}" and "T_{wi}" displays the temperature of the chamber wall on its hot gas side. "T_{wc}" indicates chamber (cold side) temperature.

maximum temperature of about 2500 K and 2550 K for both the cold side and hot gas side respectively.

The temperature at the throat is expected to be the highest because the hot gasses pass through a significantly narrow region, giving rise to both temperature and pressure.

As hot gases are released, temperatures drop sharply and marginally from the nozzle to exhaust at 2100 K. This drop is because of sudden enlargement of the nozzle size as compared to the throat and the expulsion of heat to the atmosphere.

4. Conclusions

The thruster system design in this paper detailed the basic design procedure of bipropellant propulsion engines for given spacecraft mission requirements. This procedure increases the design flexibility in bipropellant hypergolic propulsion system. The expected thrust chambers performance (100 N) obtained from our computation using thermodynamic analysis, is an ideal theoretical performance. The drop in using RPA to verify the nozzle performance indicates that a real thrust chamber is considered, where the flow is axisymmetric two-dimensional (or even three dimensional), with a viscous boundary layer next to the nozzle walls. It also occurs where the gas velocities are much lower than the core-stream velocities, finite-rate chemical kinetics, and other factors which reduce the real delivered performance. Under vacuum exit condition, there is a need to adjust the nozzle expansion ratio and chamber pressure to attain the target thrust level. By changing the ratios of the feeding of the catalyst solution and the hydrogen peroxide to the thruster, the generated thrust generated is significantly con-

trolled.

The future design process will involve selecting and sizing other elements of propulsion systems such as injectors, propellant tanks, pipelines, valves. The prototype of all the designed components will be 3D printed and assemble for operation and testing under ambient condition.

Conflicts of Interest

The authors declare no conflicts of interest regarding the publication of this paper.

References

[1] Gagne, K.R., McDevitt, M.R. and Hitt, D.L. (2018) A Dual Mode Propulsion System for Small Satellite Applications. *Aerospace* (*Basel*), **5**, 52. https://doi.org/10.3390/aerospace5020052

[2] Larsson, W.J. and Wertz, J.R. (1999) Space Mission Analysis and Design. 3rd Edition, Vol. 8, Microcosm Press and Kluwer Academic Publishers, London, 685-716.

[3] Peter, E. (2005) A Brief Introduction to Spacecraft Propulsion. http://fred.unis.no/AGF218/Handout_Erichsen_Propulsion.pdf

[4] Sutton, G.P. and Biblarz, O. (2001) Rocket Propulsion Elements. 7th Edition, Ch. 7, Sec. 7, John Wiley & Sons, New York, 263-264.

[5] Huzel, D.K. and Huang, D.H. (1992) Modern Engineering for Design of Liquid-Propellant Rocket Engines. Progress in Astronautics and Aeronautics. Vol. 147, American Institute of Aeronautics & Astronautics, Reston, 432.

[6] Koelle, H.H. (1961) Handbook of Astronautical Engineering. Section 17: Propulsion Fundamentals. McGraw-Hill Book Company, Inc., New York.

[7] Woschnak, A., Krejci, D., Schiebl, M. and Scharlemann, C. (2013) Development of Green Bipropellant Hydrogen Peroxide Thruster for Attitude Control on Satellites. *Progress in Propulsion Physics*, **4**, 689-706. https://doi.org/10.1051/eucass/201304689

[8] Othman, N., Krishnan, S., Wan-Ali, K. and Jaafar, M. (2011) Design and Testing of a 50 N Hydrogen Peroxide Monopropellant Rocket Thruster. *Jurnal Meckanikal*, No. 33, 70-81.

[9] Tsujikado, N., Koshimae, M., Ishikawa, R., Kitahara, K., Ishihara, A. and Sakai, Y. (2012) An Application of Commercial Grade Hydrogen Peroxide for Hybrid/Liquid Rocket Engine. 38*th AIAA/ASME/SAE/ASEE Joint Propulsion Conference & Exhibition*, Indianapolis, 7-10 July 2002, 2002-2007. https://doi.org/10.2514/6.2002-3573

[10] Sungkwon, J., Sungyong, A., Jonghak, K., Hosung, Y. and Sejin, K. (2011) Performance Characteristics of Hydrogen Peroxide/Kerosene Staged-Bipropellant Engine with Axial Fuel Injector. *Journal of Propulsion and Power*, **27**, 684-687. https://doi.org/10.2514/1.B34083

[11] Sutton, G. (2001) Rocket Propulsion Elements. 7th Edition, John Wiley and Sons, Hoboken, 4-13, 75-76, 268-341.

[12] Sisco, J., Anderson, W., Austin, B. and Mok, J. (2005) Autoignition of Kerosene by Decomposed Hydrogen Peroxide in a Dump-Combustor Configuration. *Journal of Propulsion and Power*, **21**, 450-459. https://doi.org/10.2514/1.5287

[13] Nothnagel, S.L. (2011) Development of Cold Gas Propulsion System for the Talaris

Hopper. Thesis, Massachusetts Institute of Technology, Department. of Aeronautics and Astronautics, Cambridge, 122-128.

[14] Ronald, W.H., Gary, N.H. and Willy, J.L. (1995) Space Propulsion Analysis and Design. Revised Edition, McGraw-Hill, New York, Ch. 1 and 3, Sec. 1.1 and 3.6, 17 and 138-145.

[15] Krzycki, L.J. (1967) How to Design, Build and Test Small Liquid-Fuel Rocket Engines. Facsimile Edition, Rocketlab, Long Beach, 12-34.

[16] Hill, P.G. and Peterson, C.R. (2014) Mechanics and Thermodynamics of Propulsion. 2nd Edition, 20th Impression, Part 3, 467-558.